Nephrol Dial Transplant (2018) 33: 1129–1137
doi: 10.1093/ndt/gfx332
Advance Access publication 22 December 2017

ORIGINAL ARTICLE

Genetic background influences cardiac phenotype in murine chronic kidney disease

Samantha Neuburg[1], Corey Dussold[1], Claire Gerber[1], Xueyan Wang[1], Connor Francis[1], Lixin Qi[1], Valentin David[1], Myles Wolf[2] and Aline Martin[1]

[1]Division of Nephrology and Hypertension, Department of Medicine, Center for Translational Metabolism and Health, Institute for Public Health and Medicine, Northwestern University Feinberg School of Medicine, Chicago, IL, USA and [2]Division of Nephrology, Department of Medicine, Duke Clinical Research Institute, Duke University, Durham, NC, USA

Correspondence and offprint requests to: Aline Martin; E-mail: aline.martin@northwestern.edu

ABSTRACT

Background. Levels of fibroblast growth factor 23 (FGF23) increase early in chronic kidney disease (CKD) and are independently associated with left ventricular hypertrophy (LVH), heart failure and death. Experimental models of CKD with elevated FGF23 and LVH are needed. We hypothesized that slow rates of CKD progression in the Col4a3 knockout ($Col4a3^{KO}$) mouse model of CKD would promote development of LVH by prolonging exposure to elevated FGF23.

Methods. We studied congenic $Col4a3^{KO}$ and wild-type (WT) mice with either 75% 129X1/SvJ (129Sv) or 94% C57Bl6/J (B6) genomes.

Results. B6-$Col4a3^{KO}$ lived longer than 129Sv-$Col4a3^{KO}$ mice (21.4 ± 0.6 versus 11.4 ± 0.4 weeks; $P < 0.05$). 10-week-old 129Sv-$Col4a3^{KO}$ mice showed impaired renal function (blood urea nitrogen 191 ± 39 versus 34 ± 4 mg/dL), hyperphosphatemia (14.1 ± 1.4 versus 6.8 ± 0.3 mg/dL) and 33-fold higher serum FGF23 levels ($P < 0.05$ versus WT for each). Consistent with their slower CKD progression, 10 week-old B6-$Col4a3^{KO}$ mice showed milder impairment of renal function than 129Sv-$Col4a3^{KO}$ mice and modest FGF23 elevation without other alterations of mineral metabolism. At 20 weeks, further declines in renal function in B6-$Col4a3^{KO}$ mice was accompanied by hyperphosphatemia and 8-fold higher FGF23 levels ($P < 0.05$ versus WT for each). Only the 20-week-old B6-$Col4a3^{KO}$ mice developed LVH (LV mass 125 ± 3 versus 98 ± 6 mg; $P < 0.05$ versus WT) in association with significantly increased cardiac expression of FGF receptor 4 (FGFR4) messenger RNA and protein and markers of LVH (Atrial natriuretic peptide (ANP), B-type natriuretic peptide (BNP), beta-myosin heavy chain (β-MHC); $P < 0.05$ versus WT for each).

Conclusions. In conclusion, B6-$Col4a3^{KO}$ mice manifest slower CKD progression and longer survival than 129Sv-$Col4a3^{KO}$ mice and can serve as a novel model of cardiorenal disease.

Keywords: chronic kidney disease, Col4a3 null mouse, FGF23, genetic background, left ventricular hypertrophy

INTRODUCTION

Fibroblast growth factor 23 (FGF23) is a bone-derived hormone that regulates phosphate homeostasis. In chronic kidney disease (CKD), disordered bone and mineral metabolism is a common complication that begins early and worsens progressively as kidney function declines. In CKD, an increased level of FGF23 is currently the earliest detectable sign of disordered mineral metabolism and a powerful risk factor for left ventricular hypertrophy (LVH), heart failure and death [1–4]. FGF23 induces LVH through direct activation of FGF receptor 4 (FGFR4) and phospholipase C gamma signaling in cardiac myocytes [5, 6] independent of its coreceptor αKlotho, which exerts cardioprotective effects [7]. However, the exposure time and concentration thresholds required for FGF23 to induce LVH *in vivo* during CKD progression are unknown. Indeed, investigation of cardiac effects of FGF23 in CKD has been limited by a lack of experimental models that recapitulate the early elevations of FGF23 levels and development of LVH that characterize human CKD.

The most frequently used CKD models involve surgical reductions of kidney function in rats and mice (i.e. 5/6 nephrectomy, unilateral ureteral obstruction, ischemia reperfusion) or administration of nephrotoxic diets (high phosphate, adenine). Surgical models are limited by substantial risk of mortality, heterogeneous effects on kidney function and the difficulty to dissociate the specific effects of kidney injury from the general effects of invasive surgery on the downstream phenotype. Although 5/6 nephrectomy can induce alterations of mineral metabolism and LVH, producing the full phenotype often necessitates dual administration of high-phosphate diets, and the amplitude of the

response does not reliably reproduce the temporal alterations in mineral metabolism observed clinically in human CKD, in which elevations of serum FGF23 occur prior to elevations of serum phosphate [8–10]. Adenine-induced kidney injury, used more often in rats than mice to study alterations in bone and mineral metabolism [11, 12], induces nephrolithiasis with extensive tubular necrosis. While some alterations of bone and mineral metabolism occur, the development of LVH has not been studied in adenine-fed mice, and the severity of the phenotype is mitigated on the C57Bl6 background [13], which is more resistant to ectopic calcification [14].

Mutations of the alpha 3 chain of type IV collagen (Col4a3) cause Alport syndrome in humans and an aggressive form of progressive CKD in mice [15, 16]. Col4a3 knockout ($Col4a3^{KO}$) mice on the 129SvX1/J genetic background show normal kidney function until about 4 weeks of age. After 4 weeks, renal function declines rapidly in association with proteinuria and exponential increases in FGF23 levels. Cardiac systolic dysfunction, end-stage renal disease and death usually occur by 9–10 weeks of age [17–20]. Hence 129SvX1/J $Col4a3^{KO}$ mice have become an important model for studying alterations of FGF23 and mineral metabolism in CKD [18, 19, 21, 22]. Interestingly, the genetic background affects the rate of CKD progression in $Col4a3^{KO}$ mice [23]. Congenic $Col4a3^{KO}$ mice backcrossed to a C57Bl6/J genetic background show delayed onset of CKD, slower disease progression and, as a result, extended lifespan to 30 weeks. Alterations in mineral metabolism have been described in $Col4a3^{KO}$ mice, both on the 129SvX1/J and a mixed genetic background; however, the impact of differential rates of CKD progression and mineral metabolism alterations on the cardiac phenotype has not been investigated. We hypothesized that slower rates of CKD progression in $Col4a3^{KO}$ mice on the C57Bl6/J background would increase the duration of exposure to elevated FGF23 and promote the development of LVH compared with $Col4a3^{KO}$ mice on the 129SvX1/J background.

MATERIALS AND METHODS

Animals

We purchased 129X1/SvJ-$Col4a3^{tm1Dec}$ mutant mice ($Col4a3^{KO}$) from Jackson Laboratory (Bar Harbor, ME, USA). We first outcrossed 129X1/SvJ heterozygotes with C57BL/6J wild-type (WT) mice. We further backcrossed the F1 heterozygotes with either strain to generate incipient congenic strains: first, for one generation with 129X1/SvJ WT mice to obtain a mixed background strain (N2) that contained 75% 129X1/SvJ genome (129Sv); second, for three generations to C57BL/6J WTs to obtain B6.129-$Col4a3^{tm1Dec}$ (N4) that contained 94% C57Bl6/J genome (B6). We maintained both newly created strains separately for more than five generations.

We recorded the age of death on 14 129Sv-$Col4a3^{KO}$ and 11 B6-$Col4a3^{KO}$ males. Based on the results of the survival analysis, we harvested WT and $Col4a3^{KO}$ samples on male littermates 1 week prior to the expected age of death of the $Col4a3^{KO}$ mice, i.e. at 10 weeks in the 129Sv and 20 weeks in the B6 mice. We included additional B6 WT and $Col4a3^{KO}$ groups at 10 weeks for age-matching comparisons with 129Sv 10-week-old mice. All studies were approved by the Institutional Animal Care and Use Committee at Northwestern University.

Serum and urine biochemistry

We collected overnight urine samples from animals housed in metabolic cages and serum samples by intracardiac exsanguination. We used a murine intact FGF23 (iFGF23) enzyme-linked immunosorbent assay (ELISA) to measure the active iFGF23 protein and a C-terminal FGF23 (cFGF23) ELISA that recognizes the full-length protein and its C-terminal cleavage fragments:measure total FGF23 (both from Immutopics, Carlsbad, CA, USA). We calculated the intact: to total FGF23 ratio as a surrogate marker of FGF23 cleavage [22, 24]. We measured parathyroid hormone (PTH) using a mouse intact ELISA (Immutopics), 1,25-dihydroxyvitamin D [1,25$(OH)_2$D] by immunoassay (Immunodiagnostic Systems, Gaithersburg, MD, USA) and calcium, phosphate, blood urea nitrogen (BUN), albumin and creatinine using colorimetric assays (Pointe Scientific, Canton, MI, USA).

Echocardiography and blood pressure

We performed echocardiography under isoflurane anesthesia 1 week prior to sacrifice (at 9 and 19 weeks of age) using a Vevo 770 High-Resolution Imaging System (VisualSonics, Toronto, ON, Canada). We used the parasternal short- and long-axis views to obtain 2-dimensional and M-mode images. We acquired at least 10 independent cardiac cycles per each experiment. We measured cardiac output, ejection fraction (EF) and stroke volume across the long axis and calculated the cardiac index using the following equation: cardiac index = cardiac output/body weight.

We measured blood pressure (BP) in sentient mice using a computerized mouse tail-cuff system (CODA, Kent Scientific, Torrington, CT, USA). We performed acquisitions for 20 cycles, once a day during three consecutive days, to familiarize each mouse with the system and to reduce environmental stress. We analyzed the third-day data from habituated mice.

Heart and kidney histology

We harvested hearts and left kidneys at sacrifice and fixed them in 100% ethanol. We recorded whole-heart weights postdehydration and normalized to tibia length to account for growth variability. We embedded hearts and kidneys in paraffin. We collected 4-μm-thick cross sections from the midchamber of the heart and 5-μm-thick longitudinal kidney sections using a rotary microtome. We stained the sections with hematoxylin and eosin (H&E) to determine cardiac and renal glomerular and tubular morphology, periodic acid–Schiff (PAS) to assess glomerular basement membrane (GBM) alterations, picrosirius red (PSR) to determine cardiac and renal fibrosis and Alexa Fluor 594 wheat germ agglutinin (WGA) conjugate to determine cardiomyocyte cross-sectional area. For cardiomyocyte cross-sectional area, we used red fluorescent microscopy (Leica Microsystems, Buffalo Grove, IL, USA) on five fields from four randomly selected heart sections (10× magnification) and calculated the sarcolemmal surface area using Leica Application Suite embedded software. For the total

Table 1. Impaired renal function in Col4a3^{KO} mice

Biochemical parameters of renal function	129Sv		B6			
	10 weeks		10 weeks		20 weeks	
	WT	Col4a3^{KO}	WT	Col4a3^{KO}	WT	Col4a3^{KO}
BUN (mg/dL)	34.1 ± 4.4	190.8 ± 38.6[b]	24.9 ± 1.2	41.2 ± 1.9[a]	24.0 ± 2.6	85.2 ± 16.9[a]
Serum creatinine (mg/dL)	0.27 ± 0.01	1.59 ± 0.40[a]	0.40 ± 0.03	1.05 ± 0.05[a]	0.50 ± 0.02	1.29 ± 0.11[a]
eGFR (μL/min)	39.6 ± 3.9	7.0 ± 1.5[b]	43.7 ± 1.7	27.2 ± 5.4[a]	45.2 ± 7.5	18.5 ± 1.5[a]
ACR (mg/mg)	1.5 ± 0.2	7.4 ± 1.7[b]	0.9 ± 0.3	3.6 ± 0.5[a]	0.7 ± 0.1	4.0 ± 1.2[a]
24-h urine albumin (ug)	149.1 ± 31.4	678.4 ± 175.7[a]	205.0 ± 75.9	848.0 ± 281.8[a]	222.1 ± 32.6	1450.6 ± 238.9[b]

Values are mean ± standard error, $n = 5$ per group.
$P < 0.05$ versus [a]WT, [b]all groups.

percentage of cardiac fibrosis, we calculated the total percentage of fibrotic area on six fields from two heart sections (20× magnification), excluding all perivascular fibrosis areas, using Image J software (National Institutes of Health, Bethesda, MD, USA).

Real-time quantitative polymerase chain reaction (PCR)

We isolated total RNA from hearts and kidneys harvested at sacrifice using TRI reagent and synthesized first-strand cDNA (iScript cDNA Synthesis Kit, Bio-Rad Laboratories, Hercules, CA, USA). We used the iCycler iQ real-time PCR detection system, iQ SYBR Green supermix (Bio-Rad Laboratories) and adequate primer pairs (Supplementary data, Table S1) for real-time quantitative PCR analysis. The threshold of detection of each gene expression was set at optimal reaction efficiency. The expression was plotted against a standard dilution curve of relative concentration, normalized to glyceraldehyde-3-phosphate dehydrogenase expression in the same sample and expressed as the fold change versus WT.

Immunohistochemistry

We dried, deparaffinized and rehydrated the heart sections. After antigen retrieval by incubation in citric acid buffer (10 mM, pH 3) for 60 min at 37°C, we blocked non-specific sites with 1X animal-free blocker (Vector Labs, Burlingame, CA, USA); we incubated sections with anti-FGFR4 primary antibody (sc-136988, Santa Cruz Biotechnology, Dallas, TX, USA) for 1 h. We used the immunohistological Vectastain ABC kit (Vector Labs) and counterstained the slides with picric acid. We used liver sections as a positive control and secondary antibody in absence of anti-FGFR4 primary antibody as a negative control. We used bright-field microscopy (Leica Microsystems, Buffalo Grove, IL, USA) to visualize FGFR4-specific black staining generated by the Vector Black alkaline phosphatase substrate kit (Vector Labs).

Statistics

Data are presented as mean ± SE. We performed Shapiro–Wilk W tests of normality on each parameter. To test statistical differences for parameters that followed a normal distribution, we used parametric analysis of variance (ANOVA) followed by *post hoc t*-tests. For all other parameters we performed Kruskal–Wallis tests followed by Mann–Whitney nonparametric tests (Statistica software, Statsoft, Tulsa, OK, USA). Differences were considered statistically significant at P-values <0.05.

RESULTS

Extended lifespan in B6-Col4a3^{KO} compared with 129Sv-Col4a3^{KO}

Consistent with previous reports [17, 23], we confirm that Col4a3^{KO} mice die prematurely compared with WT mice and that B6-Col4a3^{KO} mice have an extended lifespan compared with 129Sv-Col4a3^{KO} (∼21.4 ± 0.6 versus ∼11.4 ± 0.4 weeks; $P < 0.05$; Supplementary data, Figure S1).

Slower CKD progression in B6-Col4a3^{KO} than in 129Sv-Col4a3^{KO}

We compared the effects of genetic background on CKD severity by analyzing the kidney phenotype of WT and Col4a3^{KO} mice 1 week prior to the expected death of the Col4a3^{KO} mice: at 10 weeks in 129Sv and at 20 weeks in B6. We also analyzed 10-week-old B6 mice for direct comparison with the 10-week-old 129Sv mice. BUN, serum creatinine, albumin:creatinine ratio (ACR) and 24-h urinary albumin excretion were all significantly elevated and estimated glomerular filtration rate was significantly reduced in Col4a3^{KO} compared with WT mice, suggesting that deletion of Col4a3 induces impaired renal function and proteinuria on both genetic backgrounds (Table 1). Consistently, renal histology showed advanced glomerulosclerosis, tubular atrophy and interstitial fibrosis in 10-week-old 129Sv-Col4a3^{KO} compared with WT mice, whereas age-matched 10-week-old B6-Col4a3^{KO} mice had a much milder phenotype Supplementary data, Figure S2). The 20-week-old B6-Col4a3^{KO} kidneys also displayed extensive glomerular damage, tubular damage and tubulointerstitial fibrosis, however, 10-week-old 129Sv-Col4a3^{KO} showed the most severe kidney disease (Table 1, Supplementary data, Figure S2).

Increased FGF23 is the earliest detectable sign of disordered mineral metabolism in CKD mice

As previously published [18, 19], 129Sv-Col4a3^{KO} mice with advanced CKD showed significant elevations of serum PTH and reductions in 1,25$(OH)_2$D together with increased serum phosphate, serum calcium and fractional excretion of

Table 2. Altered mineral metabolism in Col4a3^{KO} mice

Biochemical parameters of mineral metabolism	129Sv		B6			
	10 weeks		10 weeks		20 weeks	
	WT	Col4a3^{KO}	WT	Col4a3^{KO}	WT	Col4a3^{KO}
PTH (pg/mL)	281.5 ± 35.8	2521.6 ± 675.3[a]	640.8 ± 215.8	770.2 ± 152.9	415.5 ± 62.2	3644.4 ± 1201.8[a]
1,25(OH)$_2$D (pg/mL)	76.1 ± 14.4	43.0 ± 7.4	164.7 ± 18.1[c]	170.4 ± 24.7[c]	197.2 ± 23.5[c]	203.1 ± 16.7[c]
Pi (mg/dL)	6.8 ± 0.3	14.1 ± 1.4[b]	7.0 ± 0.5	7.5 ± 0.8	6.2 ± 0.4	8.9 ± 0.8[a]
Ca^{2+} (mg/dL)	10.4 ± 0.2	12.7 ± 1.3[a]	10.5 ± 0.8	12.1 ± 0.5	7.6 ± 0.2	9.9 ± 0.5[a]
FePi (%)	6.5 ± 1.7	15.4 ± 2.7[a]	9.5 ± 2.3	17.3 ± 2.5[a]	4.8 ± 0.7	12.7 ± 1.9[a]
FeCa (%)	0.9 ± 0.4	10.6 ± 4.6[a]	0.9 ± 0.3	1.2 ± 0.1	0.6 ± 0.1	3.6 ± 1.3[a]

Values are mean ± standard error, $n = 5$ per group.
$P < 0.05$ versus [a]WT, [b]all groups and [c]all 129Sv.

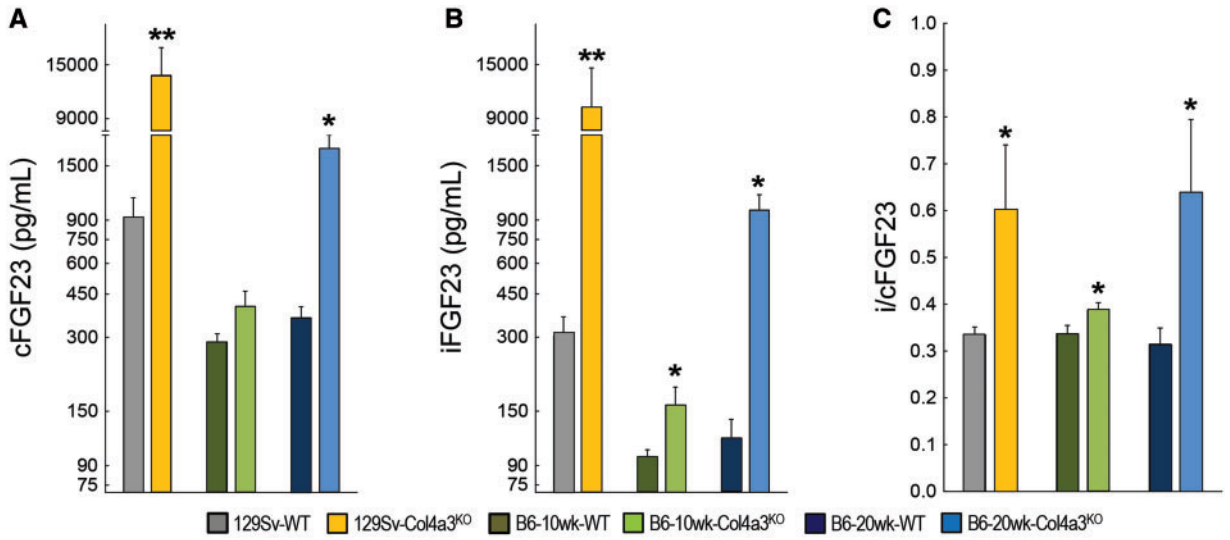

FIGURE 1: CKD induces an elevation in circulating FGF23 levels in Col4a3^{KO} mice.
Logarithmic representation of serum (**A**) total FGF23 (cFGF23), (**B**) intact FGF23 (iFGF23) and (**C**) calculated ratio of intact to total FGF23 (i/cFGF23) in 10-week-old 129Sv, 10-week-old B6 and 20-week-old B6 WT and Col4a3^{KO} mice. Values are mean ± standard error, $n = 5$ per group. $P < 0.05$ versus *WT and **all groups.

phosphate (FePi) and calcium (FeCa) compared with WT (Table 2). Also consistent with previous reports [21], they demonstrated ~90% lower messenger RNA (mRNA) expression of αKlotho in the kidney (Supplementary data, Figure S2). Circulating total FGF23, measured by cFGF23 assay, and iFGF23 were dramatically increased in 129Sv-Col4a3^{KO} mice compared with WT, and the ratio of intact to total FGF23 (i/cFGF23) was 2-fold higher in 129Sv-Col4a3^{KO} mice, suggesting that increased production and reduced cleavage of FGF23 each contributed to markedly elevated levels of biologically active iFGF23 in the CKD mice (Figure 1).

In age-matched 10-week-old B6-Col4a3^{KO} mice with early CKD, serum levels of phosphate, calcium, 1,25(OH)$_2$D and PTH remained unchanged (Table 2). Only levels of intact FGF23, i/cFGF23 and FePi showed significant elevations compared with B6-WT controls (Figure 1, Table 2), suggesting that the early increase in iFGF23 was driven primarily by reduced FGF23 cleavage (marked by increased i/cFGF23) rather than increased FGF23 production (normal cFGF23).

Compared with 20-week WT controls, 20-week-old B6-Col4a3^{KO} mice with advanced CKD showed similar alterations of mineral metabolism as those observed in 10-week-old 129Sv-Col4a3^{KO} mice, including increased PTH, hyperphosphatemia, hypercalcemia, increased FePi and increased FeCa (Table 2), albeit lower absolute values, and 50% lower expression of Klotho mRNA in the kidney (Supplementary data, Figure S2). Intact FGF23 levels and i/cFGF23 were further increased in 20- versus 10-week-old B6-Col4a3^{KO} mice, and serum cFGF23 levels increased significantly from Week 10 to 20, suggesting progressive increases in FGF23 production and progressive reductions in FGF23 cleavage as CKD advanced in B6-Col4a3^{KO} mice.

Rate of CKD progression influences cardiac phenotypes in 129Sv and B6 mice

Systolic, diastolic and mean BP were elevated in all mice with advanced CKD (129Sv at -10 weeks and B6 at -20 weeks) compared with their respective age-matched WT controls (Table 3). Despite similar BP profiles in the different CKD strains, there was a striking influence of genetic background on cardiac morphology and function. The 10-week-old 129Sv-Col4a3^{KO} mice had significantly lower cardiac output, EF and

Table 3. Elevated BP in advanced Col4a3^{KO} mice on both genetic backgrounds

Blood pressure parameters	129Sv		B6			
	10 weeks		10 weeks		20 weeks	
	WT	Col4a3^{KO}	WT	Col4a3^{KO}	WT	Col4a3^{KO}
Systolic BP (mmHg)	115 ± 4	147 ± 6[a]	134 ± 5	145 ± 1	111 ± 11	146 ± 9[a]
Diastolic BP (mmHg)	84 ± 4	108 ± 8[a]	107 ± 4	110 ± 2	82 ± 11	114 ± 6[a]
Mean BP (mmHg)	94 ± 4	120 ± 7[a]	115 ± 4	121 ± 2	92 ± 11	124 ± 7[a]

Values are mean ± standard error, $n = 5$ per group.
Noninvasive systolic, diastolic and mean blood pressure (BP).
[a]$P < 0.05$ versus WT.

Table 4. Cardiac phenotype of Col4a3^{KO} mice

Echocardiography parameters	129Sv		B6			
	10 weeks		10 weeks		20 weeks	
	WT	Col4a3^{KO}	WT	Col4a3^{KO}	WT	Col4a3^{KO}
LV mass (mg)	99.0 ± 8.7	87.5 ± 7.2	97.1 ± 9.0	89.1 ± 5.0	97. 5 ± 5.6	125.1 ± 3.1[b]
LV ID, d (mm)	3.9 ± 0.1	3.7 ± 0.1	3.8 ± 0.0	4.0 ± 0.2	3.7 ± 0.1	3.5 ± 0.3
LV AW, d (mm)	0.97 ± 0.04	0.88 ± 0.05	0.89 ± 0.03	0.83 ± 0.09	1.07 ± 0.04	1.18 ± 0.10[c]
LV PW, d (mm)	0.72 ± 0.04	0.77 ± 0.05	0.84 ± 0.10	0.72 ± 0.04	0.89 ± 0.07	1.20 ± 0.09[a]
Cardiac output (mL/min)	13.3 ± 2.0	8.8 ± 0.8[a]	16.5 ± 1.0	11.6 ± 1.5[a]	13.7 ± 1.5	13.2 ± 2.7
EF (%)	55.9 ± 3.1	49.9 ± 3.5[a]	51.3 ± 3.2	46.8 ± 8.6	55.6 ± 5.9	53.4 ± 2.7
Stroke volume (uL/beat)	31.6 ± 4.1	20.5 ± 2.2[a]	37.1 ± 1.0	26.7 ± 3.4[a]	30.9 ± 2.7	28.7 ± 6.3
Cardiac index	0.59 ± 0.07	0.52 ± 0.05	0.84 ± 0.05[c]	0.62 ± 0.09	0.52 ± 0.07	0.60 ± 0.14

Values are mean ± standard error, $n = 5$ per group.
Echocardiography analysis of left ventricular (LV) mass, internal diameter (ID), anterior wall thickness (AW), posterior wall thickness (PW) measured at diastole (d), ejection fraction (EF).
$P < 0.05$ versus [a]WT, [b]all groups and [c]all 129Sv.

stroke volume compared with 129Sv-WT mice, indicating cardiac systolic dysfunction (Table 4). Interestingly, 10-week-old 129Sv-Col4a3^{KO} mice did not show significant modifications in cardiac morphology (Table 4, Figure 2); mRNA expression of markers of hypertrophy were normal A- and B-natriuretic peptides (ANP, BNP) or reduced [β-myosin heavy chain (MHC): 4-fold] (Figure 2). Consistent with the histologic findings of increased cardiac fibrosis, mRNA expression of fibrosis markers (Col1a2, Col3a1, Col4a1, Col4a2, Col6a2, Timp1) were all significantly increased in 129Sv-Col4a3^{KO} mice (Figure 3). Of note, expression of FGFR4, which mediates the hypertrophic effects of FGF23 on cardiac myocytes [6], was significantly reduced in 129Sv-Col4a3^{KO} mice compared with WT (Figure 4).

Like the 10-week 129Sv-Col4a3^{KO} mice, cardiac output and stroke volume were similarly reduced in 10-week-old B6-Col4a3^{KO} mice compared with B6-WT mice, although absolute values were higher than in the 129Sv mice. In contrast, by 20 weeks, B6-Col4a3^{KO} mice demonstrated significant LVH marked by increases in LV mass, LV posterior wall thickness, heart weight:tibia length ratio and cross-sectional area of individual LV cardiac myocytes (Table 4, Figure 2). The 20-week-old CKD mice no longer demonstrated any evidence of systolic dysfunction compared with WT (Table 4). The LVH phenotype in the 20-week-old B6-Col4a3^{KO} mice was associated with significantly increased cardiac expression of mRNA markers of hypertrophy (BNP, β-MHC) and histological evidence of intramyocardial fibrosis with an ∼1.5-fold increase in Col4a1 and Timp1 mRNA expression (Figure 3). In sharp contrast to the 10-week-old 129Sv-Col4a3^{KO} mice that demonstrated decreased cardiac FGFR4 expression, 20-week-old B6-Col4a3^{KO} mice manifested 2-fold higher mRNA expression and increased protein expression of FGFR4 in the heart (Figure 4).

DISCUSSION

In Alport's syndrome, mutations of the alpha 3 chain of type IV collagen result in abnormal collagen assembly in the GBM, leading to impaired renal function [25, 26]. Genetic background significantly influences the rate of CKD progression in human [27] and murine Alport's syndrome [23]. Consistent with previous literature [23], we confirmed that incipient congenic strains of Col4a3^{KO} mice show distinct renal phenotypes. As expected, 94% derivation to the B6 genetic background mitigated the severity of the Col4a3 mutation on kidney function enough to lead to a longer lifespan compared with 129Sv-Col4a3^{KO} mice. While this may be caused by earlier onset of CKD in 129Sv-Col4a3^{KO} mice [16], genetic modifiers and differences in GBM composition, including assembly of α5/α6 chains of type IV collagen, which compensate for lack of α3 chains, may also contribute to slower rates of CKD progression in B6-Col4a3^{KO} mice [16, 17].

Our results indicate that both 129Sv and B6 mice with advanced CKD display clear evidence of abnormal mineral metabolism, including elevated serum FGF23 levels,

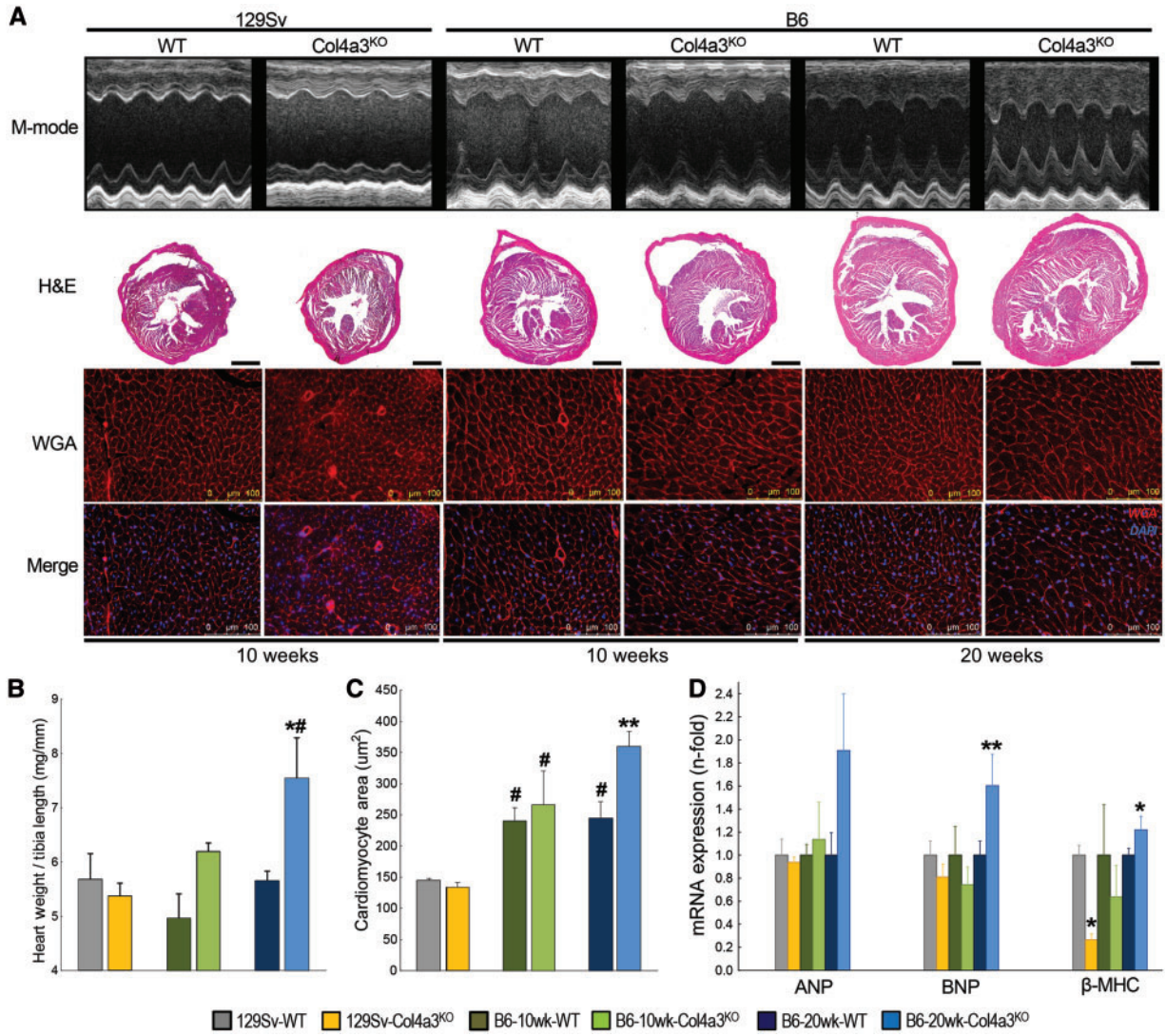

FIGURE 2: Cardiac hypertrophy only develops in slow-progressing B6-Col4a3^{KO} mice with advanced CKD. **(A)** M-mode echocardiography and representative cardiac midchamber histology in 10-week-old 129Sv, 10-week-old B6 and 20-week-old B6 WT and Col4a3^{KO} mice. Bright-field microscopy: H&E (composite, scale bar = 1 mm) staining showing cardiac morphology; fluorescence microscopy: WGA and merged WGA and DAPI staining (merge, scale bar = 100 μm) showing cardiomyocyte size and number. **(B)** Heart weight:tibia length ratio. **(C)** Cardiomyocyte cross-sectional area calculated from WGA stained sections. **(D)** Cardiac mRNA expression of markers of hypertrophy (ANP, BNP and β-MHC). Values are mean ± standard error, n = 4–7 per group. P < 0.05 versus *WT, #all 129Sv and **all groups.

hyperphosphatemia and αKlotho deficiency. Consistent with the slower disease progression, 10-week-old B6-Col4a3^{KO} mice with early CKD showed elevations of iFGF23 and FePi prior to any alterations in serum phosphate, 1,25(OH)$_2$ D or PTH. This is consistent with previous observations from human studies [2, 28], in mice with acute kidney injury [29] and in rats with CKD induced by anti-GBM antiserum [30] in which FGF23 was found to be the first detectable alteration in mineral metabolism following induction of renal injury. Here we show a similar pattern in a genetic mouse model of progressive CKD, which supports the concept that elevated iFGF23 antedates other alterations of mineral metabolism in CKD and stabilizes serum phosphate by increasing FePi.

An important new finding in this report is that only levels of iFGF23 and i/cFGF23, but not cFGF23, were significantly elevated in 10-week-old B6-Col4a3^{KO} mice with early CKD. Serum iFGF23 concentration reflects the balance between FGF23 transcription and cleavage of the newly synthesized intact protein in bone [22]. cFGF23 levels inform the amount of FGF23 transcription, whereas iFGF23 levels inform the amount of FGF23 cleavage relative to transcription. Coupling of FGF23 cleavage to transcription maintains normal circulating levels of iFGF23 in settings of high FGF23 transcription, such as iron deficiency [22, 31, 32]. However, in certain disease states, including CKD, uncoupling of FGF23 transcription and cleavage results in preferential increases in circulating iFGF23 that can be detected by high i/cFGF23 ratios [22, 24, 31]. Our finding that cFGF23 levels remained normal in 10-week-old B6-Col4a3^{KO} mice with early CKD and previous data showing increased circulating levels of intact FGF23 prior to elevation of FGF23 mRNA in bone in the same model [18] suggest that impaired or downregulated FGF23 cleavage rather than

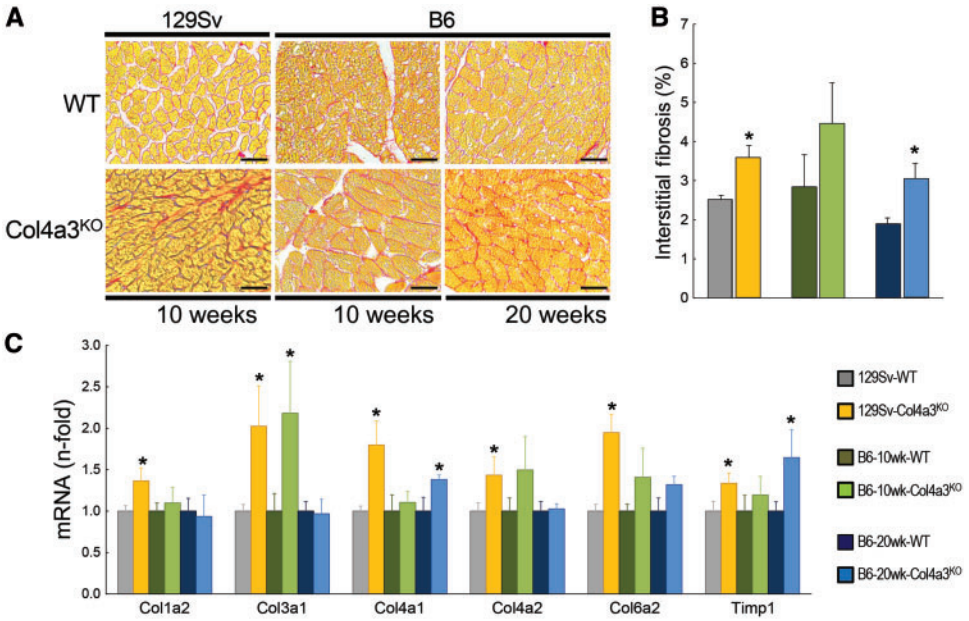

FIGURE 3: Increased cardiac fibrosis in Col4a3^{KO} mice.
(A) Bright-field microscopy of picrosirius red (PSR, scale bar = 25 μm) staining showing interstitial fibrosis, **(B)** total percent of interstitial fibrotic area calculated from PSR-stained sections and **(C)** mRNA expression of markers of fibrosis (Col1a2, Col3a1, Col4a1, Col4a2, Col6a2 and Timp1) in 10-week-old 129Sv, 10-week-old B6 and 20-week-old B6 WT and Col4a3^{KO} mice. Values are mean ± standard error, $n = 4–7$ per group. *P < 0.05 versus WT.

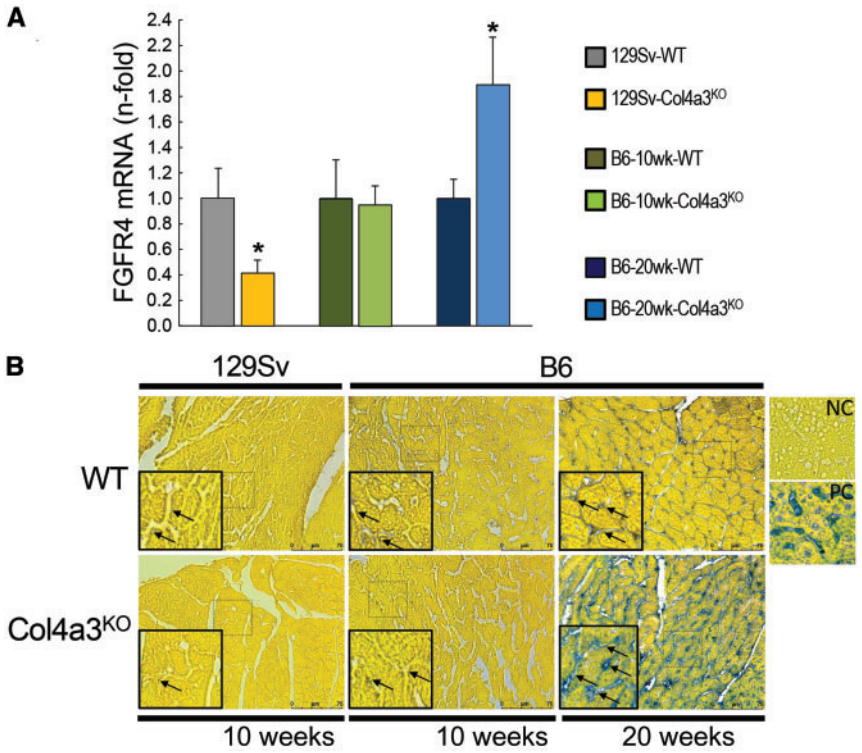

FIGURE 4: Cardiac FGFR4 expression in Col4a3^{KO} mice.
(A) mRNA expression of FGFR4 and **(B)** bright-field microscopy of FGFR4 immunohistochemistry (scale bar = 75 μm) in 10-week-old 129Sv, 10-week-old B6 and 20-week-old B6 WT and Col4a3^{KO} mice. Values are mean ± standard error, $n = 3–7$ per group. *P < 0.05 versus WT. NC, negative control; PC, positive control.

increased production is likely the initial event that increases iFGF23 levels in CKD. In contrast, both cFGF23 and iFGF23 were increased in mice with advanced CKD, suggesting that stimulation of FGF23 transcription occurs later during CKD progression to further boost circulating FGF23 levels. Additional research is needed to define the mechanisms of FGF23 cleavage in osteocytes and how this is altered by CKD.

Increased FGF23 in CKD is independently associated with increased risks of cardiovascular events and mortality [1, 2]. Because Col4a3^{KO} mice show similar alterations of mineral metabolism as observed in patients with CKD, including elevations of serum FGF23 levels, they have become an established model to study mineral metabolism in CKD on both genetic backgrounds [18, 19, 21, 22]. The fact that Col4a3^{KO} mice spontaneously develop progressive kidney disease represents a potential advantage over surgically or dietary-induced models of CKD [8–11]. However, experimental models of CKD progression that recapitulate the amplitude of alterations in mineral and the associated cardiac phenotypes observed in patients with CKD are generally lacking. Our data show that Col4a3^{KO} mice represent a novel model to advance cardiorenal research. For investigators focused on studying CKD progression or disordered mineral metabolism, the 129Sv background provides an accelerated model of disease, whereas the B6 model, despite much slower disease progression than 129Sv, provides a unique advantage for investigators focused on studying the interaction between CKD and LVH.

Col4a3 is not normally expressed in the heart [33], suggesting that downstream alterations of CKD drive the cardiac phenotype of Col4a3^{KO} mice. Both 129Sv and B6 advanced CKD mice were hypertensive and both displayed significant cardiac fibrosis. However, their cardiac phenotypes were distinct. Advanced CKD 129Sv mice showed significant cardiac dysfunction, whereas B6 mice developed LVH with normal cardiac function and improved survival. Although hypertension may have contributed to cardiac injury, its similar severity in both strains could not explain the differences observed between 129Sv- and B6-Col4a3^{KO} hearts. The reduced EF and stroke volume found in 129Sv-Col4a3^{KO} mice are consistent with prior reports on the same mice showing reduced EF and reduced fractional shortening in the absence of LVH [20]. It is also consistent with clinical reports showing increased risk of cardiac dysfunction in patients with early onset and aggressive forms of Alport's syndrome [34–38]. Here, B6-Col4a3^{KO} mice showed early signs of cardiac dysfunction that were ameliorated later in life, perhaps due to development of LVH. However, half of patients with heart failure also have a preserved left ventricular EF [39]. Therefore the association between cardiac hypertrophy and altered function is complex and whether LVH represents a compensatory cardiac remodeling response unveiled by slower CKD progression to avoid heart failure remains to be determined. Further studies on pure genetic background mice will be useful to assess the full extent of their cardiorenal phenotype, including the association between LVH and altered cardiac function.

Interestingly, both 129Sv and B6 mice with advanced CKD had elevated FGF23 levels and reduced αKlotho expression, but only B6-Col4a3^{KO} mice developed LVH. The fact that LVH was not observed in 129Sv-Col4a3^{KO} mice despite their 33-fold higher iFGF23 levels suggests that the amplitude of FGF23 elevation alone does not predict development of LVH. Additionally, the reduction in αKlotho expression was more pronounced in 129Sv- than in B6-Col4a3^{KO} mice, suggesting that the severity of αKlotho deficiency alone could not predict development of LVH. Of note, B6 mice show higher baseline levels of 1,25$(OH)_2$-D than 129Sv mice. While higher vitamin D levels in B6-Col4a3^{KO} mice might mitigate the progression of CKD, recent report suggests that the effects of 1,25$(OH)_2$D counteract the effects of FGF23 on the heart [40] and therefore would not likely explain the differences in heart phenotype between the two backgrounds. One possible mechanism is that the duration of exposure to increased iFGF23 levels may influence development of LVH. Since iFGF23 levels were already elevated in 10-week-old B6-Col4a3^{KO} mice, 20-week-old B6-Col4a3^{KO} mice with LVH would have been exposed to at least 10 continuous weeks of significantly increased iFGF23. This is in contrast with younger 10-week-old 129Sv-Col4a3^{KO} mice, which experienced such rapid CKD progression that cardiac modeling/remodeling may not have had time to compensate for cardiac dysfunction. Alternatively, cardiac FGFR4 mRNA expression was downregulated in 129Sv mice but upregulated in B6-Col4a3^{KO} mice, thereby providing more prohypertrophic FGF receptor targets for FGF23 to engage. Combined with chronic exposure to iFGF23 and Klotho deficiency, increased cardiac FGFR4 expression may have contributed to the development of LVH preferentially in B6-Col4a3^{KO} mice, consistent with prior reports [6, 40, 41].

To conclude, our data show that B6Col4a3^{KO} represents a new model for investigating cardiorenal syndromes that recapitulates more features of human CKD than 129Sv-Col4a3^{KO}, including chronic and slow progression of CKD, altered mineral metabolism and LVH. We show that iFGF23 elevation is the first alteration of mineral metabolism occurring in CKD before alterations of serum phosphate, PTH or 1,25$(OH)_2$D and that impaired FGF23 cleavage is a likely mechanism of the early iFGF23 elevations in CKD. In addition, we report that 129Sv-Col4a3^{KO} mice show amplified alterations of mineral metabolism and significant cardiac dysfunction but no LVH, perhaps due to rapidly accelerating CKD progression that culminates in early death. As elevations of BP and FGF23 and αKlotho deficiency alone could not explain the differences in cardiac function and LVH between the two strains, perhaps the chronicity of exposure to FGF23 or differential expression of FGFR4 may be key factors contributing to LVH specifically in B6-Col4a3^{KO} mice.

FUNDING

This work was supported by grants to A.M. (R01DK101730) and V.D. (R01DK102815) from the National Institutes of Health and to M.W. (15SFDRN25080331) from the American Heart Association.

SUPPLEMENTARY DATA

Supplementary data are available at ndt online.

CONFLICT OF INTEREST STATEMENT

V.D. has served as a consultant or received honoraria from Vifor and Luitpold and grant support from Keryx Biopharmaceuticals and Vifor. M.W. has served as a consultant

or received honoraria from Amag, Amgen, Akebia, Ardelyx, Diasorin, Incyte, Keryx, Pfizer and Sanofi and grant support from Shire. All authors report grants from the National Instituted of Health National Institute of Diabetes and Digestive and Kidney Diseases and the American Heart Association during the conducting of this study.

REFERENCES

1. Gutierrez OM, Mannstadt M, Isakova T *et al.* Fibroblast growth factor 23 and mortality among patients undergoing hemodialysis. *N Engl J Med* 2008; 359: 584–592
2. Isakova T, Xie H, Yang W *et al.* Fibroblast growth factor 23 and risks of mortality and end-stage renal disease in patients with chronic kidney disease. *JAMA* 2011; 305: 2432–2439
3. Isakova T, Houston J, Santacruz L *et al.* Associations between fibroblast growth factor 23 and cardiac characteristics in pediatric heart failure. *Pediatr Nephrol* 2013; 28: 2035–2042
4. Wolf M, Molnar MZ, Amaral AP *et al.* Elevated fibroblast growth factor 23 is a risk factor for kidney transplant loss and mortality. *J Am Soc Nephrol* 2011; 22: 956–966
5. Faul C, Amaral AP, Oskouei B *et al.* FGF23 induces left ventricular hypertrophy. *J Clin Invest* 2011; 121: 4393–4408
6. Grabner A, Amaral AP, Schramm K *et al.* Activation of cardiac fibroblast growth factor receptor 4 causes left ventricular hypertrophy. *Cell Metab* 2015; 22: 1020–1032
7. Hu MC, Shi M, Cho HJ *et al.* Klotho and phosphate are modulators of pathologic uremic cardiac remodeling. *J Am Soc Nephrol* 2015; 26: 1290–1302
8. Di Marco GS, Reuter S, Kentrup D *et al.* Treatment of established left ventricular hypertrophy with fibroblast growth factor receptor blockade in an animal model of CKD. *Nephrol Dial Transplant* 2014; 29: 2028–2035
9. Zou H, Zhao X, Sun N *et al.* Effect of chronic kidney disease on the healing of titanium implants. *Bone* 2013; 56: 410–415
10. Hofman-Bang J, Martuseviciene G, Santini MA *et al.* Increased parathyroid expression of klotho in uremic rats. *Kidney Int* 2010; 78: 1119–1127
11. Ferrari GO, Ferreira JC, Cavallari RT *et al.* Mineral bone disorder in chronic kidney disease: head-to-head comparison of the 5/6 nephrectomy and adenine models. *BMC Nephrol* 2014; 15: 69
12. Jia T, Olauson H, Lindberg K *et al.* A novel model of adenine-induced tubulointerstitial nephropathy in mice. *BMC Nephrol* 2013; 14: 116
13. Rabe M, Schaefer F. Non-transgenic mouse models of kidney disease. *Nephron* 2016; 133: 53–61
14. Qiao JH, Xie PZ, Fishbein MC *et al.* Pathology of atheromatous lesions in inbred and genetically engineered mice. Genetic determination of arterial calcification. *Arterioscler Thromb* 1994; 14: 1480–1497
15. Lemmink HH, Schroder CH, Monnens LA *et al.* The clinical spectrum of type IV collagen mutations. *Hum Mutat* 1997; 9: 477–499
16. Cosgrove D, Kalluri R, Miner JH *et al.* Choosing a mouse model to study the molecular pathobiology of Alport glomerulonephritis. *Kidney Int* 2007; 71: 615–618
17. Kang JS, Wang XP, Miner JH *et al.* Loss of alpha3/alpha4(IV) collagen from the glomerular basement membrane induces a strain-dependent isoform switch to alpha5alpha6(IV) collagen associated with longer renal survival in Col4a3-/- Alport mice. *J Am Soc Nephrol* 2006; 17: 1962–1969
18. Stubbs JR, He N, Idiculla A *et al.* Longitudinal evaluation of FGF23 changes and mineral metabolism abnormalities in a mouse model of chronic kidney disease. *J Bone Miner Res* 2012; 27: 38–46
19. Dai B, David V, Alshayeb HM *et al.* Assessment of 24,25$(OH)_2$D levels does not support FGF23-mediated catabolism of vitamin D metabolites. *Kidney Int* 2012; 82: 1061–1070
20. Touchberry CD, Green TM, Tchikrizov V *et al.* FGF23 is a novel regulator of intracellular calcium and cardiac contractility in addition to cardiac hypertrophy. *Am J Physiol Endocrinol Metab* 2013; 304: E863–E873
21. Dai B, David V, Martin A *et al.* A comparative transcriptome analysis identifying FGF23 regulated genes in the kidney of a mouse CKD model. *PLoS One* 2012; 7: e44161
22. David V, Martin A, Isakova T *et al.* Inflammation and functional iron deficiency regulate fibroblast growth factor 23 production. *Kidney Int* 2016; 89: 135–146
23. Andrews KL, Mudd JL, Li C *et al.* Quantitative trait loci influence renal disease progression in a mouse model of Alport syndrome. *Am J Pathol* 2002; 160: 721–730
24. Martin A, David V, Li H *et al.* Overexpression of the DMP1 C-terminal fragment stimulates FGF23 and exacerbates the hypophosphatemic rickets phenotype in Hyp mice. *Mol Endocrinol* 2012; 26: 1883–1895
25. Antignac C. Molecular genetics of basement membranes: the paradigm of Alport syndrome. *Kidney Int Suppl* 1995; 49: S29–S33
26. Hudson BG, Reeders ST, Tryggvason K *et al.* Collagen: structure, gene organization, and role in human diseases. Molecular basis of Goodpasture and Alport syndromes and diffuse leiomyomatosis. *J Biol Chem* 1993; 268: 26033–26036
27. Deltas C, Pierides A, Voskarides K. Molecular genetics of familial hematuric diseases. *Nephrol Dial Transplant* 2013; 28: 2946–2960
28. Wolf M. Forging forward with 10 burning questions on FGF23 in kidney disease. *J Am Soc Nephrol* 2010; 21: 1427–1435
29. Christov M, Waikar SS, Pereira RC *et al.* Plasma FGF23 levels increase rapidly after acute kidney injury. *Kidney Int* 2013; 84: 776–785
30. Hasegawa H, Nagano N, Urakawa I *et al.* Direct evidence for a causative role of FGF23 in the abnormal renal phosphate handling and vitamin D metabolism in rats with early-stage chronic kidney disease. *Kidney Int* 2010; 78: 975–980
31. Wolf M, White KE. Coupling fibroblast growth factor 23 production and cleavage: iron deficiency, rickets, and kidney disease. *Curr Opin Nephrol Hypertens* 2014; 23: 411–419
32. Farrow EG, Yu X, Summers LJ *et al.* Iron deficiency drives an autosomal dominant hypophosphatemic rickets (ADHR) phenotype in fibroblast growth factor-23 (Fgf23) knock-in mice. *Proc Natl Acad Sci USA* 2011; 108: E1146–E1155
33. Mariyama M, Leinonen A, Mochizuki T *et al.* Complete primary structure of the human alpha 3(IV) collagen chain. Coexpression of the alpha3(IV) and alpha4(IV) collagen chains in human tissues. *J Biol Chem* 1994; 269: 23013–23017
34. Earl TJ, Khan L, Hagau D *et al.* The spectrum of aortic pathology in alport syndrome: a case report and review of the literature. *Am J Kidney Dis* 2012; 60: 821–822
35. Bassareo PP, Marras AR, Mercuro G. Ventricular septal defect in a child with Alport syndrome: a case report. *BMC Cardiovasc Disord* 2010; 10: 48
36. Ferrari F, Nascimento P, Jr, Vianna PT. Complete atrioventricular block during renal transplantation in a patient with Alport's syndrome: case report. *Sao Paulo Med J* 2001; 119: 184–186
37. Sasaki N, Joashi UC, Vergara M *et al.* Postrenal biopsy AVM leading to severe hypertension and dilated cardiomyopathy. *Pediatr Nephrol* 2009; 24: 2459–2462
38. Ghosh S, Singh M, Sahoo R *et al.* Alport syndrome: a rare cause of uraemia. *BMJ Case Rep* 2014; 2014; bcr2013201731
39. Owan TE, Hodge DO, Herges RM *et al.* Trends in prevalence and outcome of heart failure with preserved ejection fraction. *N Engl J Med* 2006; 355: 251–259
40. Leifheit-Nestler M, Grabner A, Hermann L *et al.* Vitamin D treatment attenuates cardiac FGF23/FGFR4 signaling and hypertrophy in uremic rats. *Nephrol Dial Transplant* 2017; 32: 1493–1503
41. Leifheit-Nestler M, Grosse Siemer R, Flasbart K *et al.* Induction of cardiac FGF23/FGFR4 expression is associated with left ventricular hypertrophy in patients with chronic kidney disease. *Nephrol Dial Transplant* 2016; 31: 1088–1099

Received: 19.6.2017; Editorial decision: 3.11.2017